Dynamics of CO₂ dissociative chemisorption on W(110)

Rongrong Yin and Hua Guo*

Department of Chemistry and Chemical Biology, University of New Mexico,

Albuquerque, NM 87131, USA

^{*:} corresponding author: hguo@unm.edu

Abstract

We report the first globally accurate high-dimensional potential energy surface for describing the CO₂ adsorption and dissociative chemisorption on a W(110) surface based on machine learning of density functional theory data. The dissociative sticking probabilities are obtained by a quasi-classical trajectory method on the new potential energy surface and they show that reactivity is strongly enhanced by the incidence translational energy of the impinging CO₂. The CO₂ vibrational modes also enhance the reactivity but with a lesser extent. The mode specificity is understood in terms of the sudden vector projection model, in which the mode specific enhancement is attributed to differing levels of coupling with the reaction coordinate at the two transition states. In addition, the surface temperature is found to have a limited effect on the reactivity of CO₂ dissociation.

I. Introduction

Carbon dioxide is recognized as a primary anthropogenic greenhouse gas that brings a negative impact on climate changes.¹ On the other hand, CO₂ represents a highly functional and abundant chemical reagent that could potentially be a renewable and environmentally friendly source of carbon. One promising and practical way to mitigate the increasing CO₂ emissions is the catalytic reduction of CO₂ into value-added chemicals, such as carbon monoxide, methanol, ethylene and formic acid.²⁻³ Thanks to its chemical stability, the large-scale conversion of CO₂ remains a challenge and a great deal of research effort has been devoted to this field for its potential advantages. Among the various approaches explored, the process of dissociative chemisorption (DC) of CO₂ to form adsorbed CO and O on surface has long been of interest because of its role in many important industrial heterogenous catalytic reactions, such as reverse water-gas shift reaction⁴ and dry reforming of methane.⁵

However, it is well known that the activation of CO₂ on metal surfaces is challenging due to its high stability and low adsorption energy.⁶ As a result, the breaking of the C-O bond is often associated with a very high barrier.⁷⁻¹⁰ On the Pt(111) surface, for example, the barrier for CO₂ DC is close to 1.5 eV,¹¹⁻¹² making it nearly impossible for thermally activation. Even for Ni(100), where the DC barrier is very low (0.23 eV) as calculated using density functional theory (DFT),⁷ the sticking probability for CO₂ is quite small (~10⁻²).¹³ Comparably low sticking probabilities have also been reported on Si(111)-7×7, even when the incidence kinetic energy is as high as 1.5 eV.¹⁴ This is because of the very tight nature of the reaction barrier between the chemisorbed CO₂,

which has a bend geometry, and the dissociation products. 15-16

To overcome the chemical barrier, excitation of various vibrational modes of the impinging CO₂ has been proposed as a mean to enhance the reactivity. ^{13, 15-16} A detailed understanding of the reaction dynamics has benefited from the rapid development of experimentally techniques for depositing energy to specific mode(s) of the molecular reactant. 17-18 Quantum state selective measurements of reactivity based on molecular beam techniques allowed the determination of the relative efficacy of various forms of energy in promoting the DC process. 19-20 For example, in the CH₄ DC on a Ni(111) surface, the asymmetric C-H stretch vibrational mode (v₃) was found to be a more effective than translational excitation in promoting the reactivity.²¹ The mode specificity underscores the dynamical nature of the reaction in which the coupling of the reactant vibrational mode with the reaction coordinate at the transition state is strong.²² For CO₂ DC on Ni(100), enhancement of the reactivity was predicted by theoretical calculations by imparting both the translational and vibrational energy, although the efficacy is relatively low. 15-16, 23-24 However, our calculated sticking probabilities are significantly smaller than those reported in Ref. 13. Caveats have also been discussed by Burghaus concerning a number of experimental issues.²⁵

To explore other alterative surfaces in activating CO₂, we have recently undertaken an exhaustive survey of the adsorption and dissociation pathway of CO₂ on various transition metal surfaces using DFT and identified several candidates for facile CO₂ DC, such as tungsten, thanks to their ability to transfer electrons to the adsorbate.²⁶ Physisorption of CO₂ at a low temperature (<120 K) has been reported on W(011),

which also found adsorbed Na promotes the chemisorption of the molecule.²⁷ Although the decomposition of CO₂ has been reported on a tungsten surface at high temperatures,²⁸ no collision induced dissociative adsorption has been investigated. In this work, we develop a high-dimensional potential energy surface (PES) based on DFT data and explore the vibrational state specific DC dynamics of CO₂ on the W(110) surface with a quasi-classical trajectory (QCT) method. Our results indicate that the DC reaction is activated by both the translational and vibrational excitation of the impinging CO₂, and the translational excitation is more effective than vibrational excitation. Using the sudden vector projection (SVP) model,²⁹ the mode specific behaviors of the reactivity are rationalized by the strength of coupling with the reaction coordinate at each transition state. In addition, we also discussed the influence of surface temperature on the dissociative sticking probability. These theoretical predictions offer insights into the complex surface reaction dynamics of this key heterogeneous catalytic process.

II. Computational details

II. A. Density Functional Theory and Data Sampling

All periodic density functional theory (DFT) calculations were performed with the Vienna Ab initio Simulation Package (VASP).³⁰⁻³¹ The Perdew-Burke-Ernzerhof (PBE) functional³² within the generalized gradient approximation (GGA) was used to describe the exchange-correlation interaction. The electron-ion interactions were represented by the projector augmented wave (PAW) method.³³ All calculations were performed without spin polarization.

Tungsten is a body centered cubic metal, and its 110 facet is the most flat and compact one. The W(110) surface was modeled by a four-atomic-layer slab, which has a (3×3) unit cell with the top three layers relaxed, separated by a 20 Å vacuum space to avoid the inter-slab interaction. A total of 36 surface atoms are included in the unit cell, while atoms in the bottom layer are fixed at their equilibrium positions. The Brillouin zone integration was performed on a $4 \times 4 \times 1$ Monkhorst-Pack k-point mesh. The dipole correlation in the z direction was imposed to avoid the interaction between the vertically repeated images. The wave function of the valence electrons was expanded using plane waves with an energy cutoff of 400 eV. Fermi smearing with a width parameter of 0.1 eV was used. The geometries were optimized using a conjugate-gradient method until the forces acting on each atom were less than 0.02 eV/Å. The saddle points were determined using the climbing image nudged elastic band (CI-NEB)³⁴ and the dimer method, 35 and confirmed by frequency calculations.

We calculated the adsorption energies according to the following equation: $E_{\text{ads}} = E_{\text{adsorbate/slab}} - (E_{\text{adsorbate}} + E_{\text{slab}})$, where $E_{\text{adsorbate/slab}}$, $E_{\text{adsorbate}}$, E_{slab} , are the energies of the adsorbed system, the gas-phase molecule, and the bare surface, respectively.

The CO₂ + W(110) coordinate system for describe the CO₂ DC process is schematically illustrated in Figure 1, in which the molecule configuration is determined by the C-O1 bond length (r_{CO1}), C-O2 bond length (r_{CO2}), the bond angle of the two C-O bonds (\angle O1CO2), the distance of the molecular center of mass (COM) to surface (r_{CCOM}), and the polar angle (r_{CO1}) and azimuthal angle (r_{CO2}). A total of 30 mobile atoms are included in our model, which leads to 90 degrees of freedom.

To construct the high-dimensional PES for the CO₂ + W(110) system, ab initio molecular dynamics (AIMD) simulations were initially performed to sample the configuration space. The clean surface configurations were taken from equilibrated canonical (NVT) AIMD snapshots of the clean surface at surface temperature $T_s=350$ K and 650 K. Microcanonical AIMD trajectories were initiated with CO₂ being far above the W(110) surface ($z_{\text{COM}}=6.0 \text{ Å}$) with incidence energies $E_i=0.31$ and 0.5 eV and velocity pointing towards the surface along the surface normal. The initial lateral positions and orientations of the CO₂ molecule were selected randomly covering the unit cell. The CO₂ molecule is prepared with different vibrational energies associated with different normal mode quantum numbers (v_{ss} , v_b , v_{as}), for which the atomic cartesian coordinates and momenta are sampled from the normal modes. On the other hand, the rotational angular momentum of the impinging molecule was assumed to 0. These AIMD trajectories were propagated using the leapfrog algorithm in VASP with a time step of 1 fs, up to a maximum propagation time of 10 ps. A trajectory was classified as "reactive" if one of the C-O distances became larger than 2.5 Å, while as "scattered" if the molecule was flying away from the surface by 6.0 Å. Otherwise, the trajectory was labeled as "trapped" and terminated after 10 ps.

We first selected ~7000 points out of ~270000 points from ~290 micro-canonical AIMD trajectories, according to their generalized Euclidian distances (GED) in terms of inter-nuclear distances and atomic forces.³⁶ These points were fitted to a preliminary PES, using a machine learning method described below. The PES enabled QCT calculations for different vibrational quantum numbers of CO₂ molecules impinging at

W(110) surface. New data points from these trajectories were selectively included into the data set based on the same GED criterion so that they were not too close to existing points. The augmented data set was then used to update the PES, followed by a new iteration of trajectory calculations. This process was repeated until the dissociative sticking probabilities of CO₂ was converged.

II. B. Neural Network Potential Energy Surface

The AIMD approach is a powerful tool to explore the reaction dynamics, but is computationally expensive due to the repeated DFT calculations along the trajectories, especially for long time dynamics. A more efficient way to characterize the dynamics is to replace the DFT calculations using a machine learned high dimensional PES.³⁷⁻³⁸ Such PESs are necessarily high-dimensional because a sufficient number of surface atoms have to be included to account for the energy transfer accompanying the collision process.³⁹ The CO₂ + W(110) PES was constructed by means of the embedded atom neural network (EANN) approach.⁴⁰ In the EANN framework, the total energy of the system is regarded as the sum of atomic energies, each of which is an output of an atomic NN determined by the electron density of this atom embedded in the environment consisting of other atoms nearby,⁴⁰

$$E = \sum_{i=1}^{N} E_i = \sum_{i=1}^{N} NN_i \left(\boldsymbol{\rho}^i \right). \tag{1}$$

For simplicity, the embedded electron density like structural descriptors ($\boldsymbol{\rho}^{l}$) can be represented by Gaussian-type orbitals (GTOs) centered at neighboring atoms, resulting in multiple orbital-dependent density components,

$$\rho_{L,\alpha,r_s}^{i} = \sum_{l_x,l_y,l_z}^{l_x+l_y+l_z=L} \frac{L!}{l_x!l_y!l_z!} \left(\sum_{j=1}^{n_{atom}} c_j \varphi_{l_x l_y l_z}^{\alpha,r_s} \left(\mathbf{r}_{ij}\right) f_c(r_{ij})\right)^2, \tag{2}$$

where n_{atom} is the total number of atoms lying nearby the embedded atom within a cutoff radius (r_c) and $f_c(r_{ij})$ a cutoff function⁴¹ to ensure that the contribution of each neighbor atom decays smoothly to zero at r_c . The GTO is written as,

$$\varphi_{l_x l_y l_z}^{\alpha, r_s} \left(\mathbf{r}_{ij} \right) = x^{l_x} y^{l_y} z^{l_z} \exp\left(-\alpha \left| r_{ij} - r_s \right|^2 \right), \tag{3}$$

where \mathbf{r}_{ij} =(x, y, z) represents the Cartesian coordinates of the embedded atom i with atom j being the origin, r_{ij} is the distance of atom i and j, l_x , l_y and l_z represent the angular momentum components in each axis, and their sum is the total orbital angular momentum (L), α and r_s are parameters that determine radial distributions of GTOs. Note that c_j in Eq. (2) serves like an element-dependent expansion coefficient of an atomic orbital for atom j, which is optimized together with the element-dependent NN parameters. The EANN PES is invariant with respect to translation, rotation, and permutation.⁴⁰ The key advantage of this EANN method is that the density-like descriptors given in Eq. (2) scale linearly with respect to the number of neighboring atoms.⁴²

The final CO₂ + W(110) PES was fitted to 9418 points with both energies and forces. These data points were divided into training and test sets with the ratio of 90:10. The hyperparameters of GTOs were L=0, 1, 2, r_c =6.0 Å, α =0.6 Å⁻², and Δr_s =0.58 Å, resulting in 33 structural descriptors. Each atomic NN consists of two hidden layers with 50 and 60 neurons in each.

II. C. Quasi-Classical Trajectory Calculations

QCT calculations were performed with the VENUS code⁴³ which is heavily

modified by us. 44 As in the AIMD calculations, the initial surface configurations were sampled randomly from a NVT run of the surface at the target surface temperature T_s =350 and 650 K. The initial CO₂ molecule was launched from 6.0 Å above the W(110) surface, whose orientation and position in the unit cell were sampled randomly. The CO₂ molecules were allowed to collide with the surface along the surface normal with the initial translational energy ranging from 0.05 to 0.65 eV. The classical rotational angular momentum (\vec{j}) was acted on the molecule given by $\vec{j} = \sqrt{J(J+1)}\hbar$, where Jis the rotational quantum number. In our QCT calculations, the CO₂ molecule is assumed to be non-rotating. Several different initial vibrational states of CO2 were prepared to understand the mode specificity and the corresponding atomic coordinates and momenta were sampled with the standard normal mode sampling scheme. These vibrational states are denoted by three normal mode quantum numbers (v_{ss} , v_b , v_{as}) for the symmetric stretching, (doubly degenerate) bending, and asymmetric stretching modes. Each trajectory was propagated via the velocity Verlet algorithm in QCT with a time step of 0.1 fs, up to a maximum propagation time of 10 ps. The trajectory was terminated and labeled as "reactive" when one of the C-O bond lengths became larger than 2.5 Å, or "scattered" when the molecule was flying away from the surface by 6.0 Å. Otherwise, the trajectory was labeled as "trapped" and terminated after 10 ps.

III. Results and discussion

Firstly, let us check the reliability of the EANN PES. The RMSEs of the total energies and atomic forces for training and validation sets were found to be 24.59 /

31.79 meV, and 43.94 / 58.85 meV/Å, respectively. Moreover, to illustrate the fitting quality, we compared in Figure 2 the energies and geometries of stationary points along the minimum energy path (MEP) for CO₂ DC process on the W(110) surface optimized with DFT and EANN PES. The barrier energy, adsorption well depth, and reaction energy are all well reproduced in EANN PES within 20 meV. The EANN PES also reproduces well the stationary point geometries (with a maximum deviation of 0.03 Å), as shown in the Figure 2.

Similar to CO₂ adsorption on Ni(100), ¹⁵⁻¹⁶ our results indicate there are two adsorption wells on W(110). The physisorbed state on W(110) features a linear adsorbate loosely bound to the surface, with an adsorption energy of only 0.03 eV. The geometry of the adsorbate is almost identical to its isolated form, consistent with the weak interaction with the surface.²⁷ We note that this number might not be accurate as the PBE functional used in the DFT calculations does not include van der Waals corrections. In the chemisorption state, however, a bent CO₂* with a ∠O1CO2 angle of 108.9° adsorbed strongly with the surface, with an adsorption energy of 1.32 eV. However, the configuration of the chemisorbed CO₂ on the W(110) is somehow different from that on Ni(100).26 Instead of a bidentate adsorption configuration on Ni(100), 15-16 the CO₂ adsorbate forms a tridentate configuration, occupying a LB (long bridge) site with two O atoms at two neighboring SB (short bridge) sites, as shown in Figure 2. The energy of the chemisorption well is also significantly lower than the physisorption well, thanks to the small work function of tungsten, which leads to facile electron transfer from the metal to the adsorbate.²⁶

The subsequent dissociation starts with a tridentate bent CO₂ and reaches TS when the spectator CO moiety rotates to break its O-metal bond, while the O atom migrates from the SB site to a nearby SB site. During this process, the OC-O distance is elongate from 1.39 Å to 1.70 Å. Finally, the dissociation state features the CO* adsorbs at the top site and the O* near the hollow site.

From the MEP in Figure 2, we can see that there are two main transition states for the CO₂ DC process. At TS1, the CO₂ moiety is slightly bent (∠O1CO2=161.7°), connecting the physisorbed linear-CO₂* to the chemisorbed bent-CO₂* with a barrier of ~0.1 eV. The geometry of TS1 resembles the linear-CO₂* and locates in the entrance channel, so this is an "early" barrier. The second barrier (TS2) connects the chemisorbed bent-CO₂* with the co-adsorbed CO* and O* with the barrier is ~0.2 eV. This saddle point features a C–O bond length (1.25 Å) near its equilibrium value (1.19 Å) in spectator CO, while the other C–O bond is elongated to 1.71 Å and the O–C–O angle is 114.2°, implying a "late" barrier.

The reaction path shown in Figure 2 suggests that the DC of CO₂ on W(110) is largely controlled by TS1. Once passed the initial TS, the CO₂ adsorbate is expected to gain a significantly amount of energy, as the chemisorption well is quite deep. In addition, the chemical TS (TS2) is rather low comparing with the energy release, so the DC of CO₂ over TS2 is also expected to be facile. In other words, TS2 has a limited impact on the DC dynamics. These expectations are borne out by the dynamical calculations discussed below and consistent with observed near complete dissociation of CO2 adsorbed on a tungsten surface at high temperatures.²⁸

In the Figure 3, we display the PES contours as a function of the distance between O and the COM of non-dissociative CO ($d_{\text{CO1-O2}}$) and the CO₂ molecular COM height above the surface (z_{COM}), with the molecular x_{COM} and y_{COM} fixed at the TS2 geometry and the other coordinates optimized. Since TS1 is located at the different site and orientation, the saddle point in the Figure 3 (TS1') is a second-order saddle point actually, but its geometric character is close to that of TS1. As discussed above, the two saddle points are located in different locations along the MEP and have differing impact on the reaction probability as discussed below.

Using the EANN PES, the DC dynamics of CO₂ on the W(110) surface was investigated using a QCT method. We show in Figure 4 the initial state specific dissociative zero coverage sticking probabilities (S_0) for normal incidence as a function of incidence translational energy and total energy at two different surface temperatures T_s =350 and 650 K. Over 4000 trajectories were computed at each incidence energy to converge the final dynamics results with good statistics. Here, the total energy equals to the sum of translational, rotational and vibrational energies. Note that the sticking probabilities have almost no threshold and are quite large, very different from those on Ni(100). ¹⁵⁻¹⁶ The lack of a significant threshold is consistent with the low barrier shown in Figure 2, and the facile dissociation of CO₂ on W(110) suggests the absence of strong dynamical bottleneck. The large sticking probability is consistent with the earlier experimental observations of high temperature decomposition of CO₂ adsorbed on tungsten. ²⁸

Figure 4 clearly shows that the DC reactivity is strongly enhanced by incidence

translation energy, as S_0 increases monotonically and significantly with the incidence kinetic energy. To a lesser extent, excitations of all CO₂ vibrational modes, denoted by three normal mode quantum numbers (v_{ss} , v_b , v_{as}), also promote the DC reaction, as evidenced by the higher values of S_0 with vibrational excitations. We note in passing that there are two degenerate bending modes in this linear molecule, but in our approximate treatment they are considered as an effective single mode. In other words, $v_b=1$ and 2 correspond to one and two quanta in these modes.

To properly assess the promotional efficacies of various molecular modes, one need to compare the reactivity in terms of the total energy. From the Figure 4(c)(d), we can find that translational excitation is superior to all other forms of energy in promoting the DC of CO₂ and the bending mode is the most effective vibrational mode. On the other hand, the asymmetric stretching mode has the lowest efficacy. This is because it has the highest frequency, about 1000 cm⁻¹ higher than the symmetric stretching counterpart and ~2000 cm⁻¹ higher than the bending one, but its promoting effect is similar to the other modes. These results are somehow different from the CO₂ DC process on Ni(100) surface, 15-16 where the dissociation is strongly enhanced by translational excitation at low incidence energies but by vibrational excitation at higher energies. That behavior was attributed to the roughly the same energy of the two transition states. In the presence case, TS2 has a much lower energy, the chemisorbed CO₂ gains much energy and readily dissociates once formed, while the formation of the chemisorbed CO₂ is largely controlled by TS1, as alluded to above.

To understand the origin of the mode specificity observed in the CO₂ DC process

we relied on the sudden vector projection (SVP) model,²⁹ in which projections of the reactant vectors onto the reaction coordinate at the transition state are taken as their abilities for promoting the reactivity. The SVP model has been successfully used to predict the mode specificity in CO₂ DC process on the Ni(100) surface.¹⁵ As shown in Table I, the SVP values for the "early" barrier TS1 suggest that the translational mode along the surface normal direction (*z*) is the most effective one, and the bending mode is the most effective mode among the vibrational modes, which explain the QCT results discussed above. The SVP values for TS2 are also listed in the Table I, which suggest that the vibrational modes are more efficacious than translational mode. However, as we mentioned above, the barrier at TS2 is sufficiently small and the energy of the chemisorbed CO₂ is sufficiently low that this barrier does not serve as a bottleneck for the dissociation.

To confirm this hypothesis, we calculated the capture probabilities of CO_2 formation over the TS1. The capture probability is defined as the number of trajectories that pass over TS1 and enter the chemisorption well over the total number of trajectories. In Figure 4, it is seen that the behavior of capture probability (C_0) and dissociative sticking probability (S_0) are highly resemblant. Thus, the SVP results and the QCT results confirm that the CO_2 DC process on the W(110) surface is dominated by "early" barrier TS1 and the translational energy along surface normal is the most effective in promoting the reaction.

In Figure 5, we examine the influence of the surface temperature on the S_0 of CO_2 on W(110). It is clear from the figure that the surface temperature has a limited effect

on the sticking of CO₂, similar to what was found for CO₂ DC on Ni(100).¹⁶ This can be attributed to the small displacement of surface atoms in TS1 geometry (~0.002 Å). In other words, the thermal fluctuation of surface atoms does not lower the TS, leading to the absence of surface temperature dependence. This case is very different from the CH₄ DC which is typically affected by the surface temperature, thanks to the large displacement of one surface atom at the transition state.⁴⁵

IV. Conclusions

In summary, we present here an extensive investigation of CO₂ DC dynamics on W(110), using QCT on a globally accurate high-dimensional EANN PES. The tungsten surface behaves very different from Pt and Ni surfaces by effective promoting dissociation of CO₂. This facile DC of the greenhouse gas is unique and can be attributed to the small work function of tungsten which favors the injection of electrons into the adsorbate molecule. Based on the calculated barriers on this other facets of tungsten,²⁶ it can be expected that the DC of CO₂ would also be facile.

The QCT results show that reactivity is enhanced by both the translational excitation and all CO₂ vibrational modes, and the translational energy along the surface normal is the most efficacious. Among the vibrational modes, the bending seems to have the strongest capacity to enhance the dissociation, but the efficacy is relatively small. The situation here is very different from dissociation of methane⁴⁵ and water,²² which is dominated by a single transition state. On W(110), there are two transition states along the reaction path and the dynamics is controlled by the first one between

the physisorption well and chemisorption well, as the chemical transition state is low in energy and has a minor effect on the dissociation. Using the Sudden Vector Projection model, the behavior of various reactant modes in promoting the reactivity is rationalized by couplings with the reaction coordinate at the first transition state. In addition, we also find that the surface temperature has a limited effect on the reactivity of CO₂ dissociation. At present, the experimental research about this system is absent, but we hope the results and insights provided by the current work will inspire future experimental exploration of this important process. As discussed in our recent work,²⁶ there are several other candidates that might also be amenable for CO₂ dissociation, which should be explored.

Acknowledgements: This work is supported by the National Science Foundation (CHE-1951328). The computations were performed at the Center for Advanced Research Computing at UNM.

References

- 1. Haszeldine, R. S. Carbon capture and storage: How green can black be? *Science* **2009**, *325* (5948), 1647-1652.
- 2. Arakawa, H.; Aresta, M.; Armor, J. N.; Barteau, M. A.; Beckman, E. J.; Bell, A. T.; Bercaw, J. E.; Creutz, C.; Dinjus, E.; Dixon, D. A.; Domen, K.; DuBois, D. L.; Eckert, J.; Fujita, E.; Gibson, D. H.; Goddard, W. A.; Goodman, D. W.; Keller, J.; Kubas, G. J.; Kung, H. H.; Lyons, J. E.; Manzer, L. E.; Marks, T. J.; Morokuma, K.; Nicholas, K. M.; Periana, R.; Que, L.; Rostrup-Nielson, J.; Sachtler, W. M. H.; Schmidt, L. D.; Sen, A.; Somorjai, G. A.; Stair, P. C.; Stults, B. R.; Tumas, W. Catalysis research of relevance to carbon management: Progress, challenges, and opportunities. *Chem. Rev.* **2001**, *101* (4), 953-996.
- 3. Khodakov, A. Y.; Chu, W.; Fongarland, P. Advances in the development of novel cobalt Fischer–Tropsch catalysts for synthesis of long-chain hydrocarbons and clean fuels. *Chem. Rev.* **2007**, *107* (5), 1692-1744.
- 4. Dietz, L.; Piccinin, S.; Maestri, M. Mechanistic Insights into CO₂ activation via reverse water–gas shift on metal surfaces. *J. Phys. Chem. C* **2015**, *119* (9), 4959-4966.
- 5. Jang, W.-J.; Shim, J.-O.; Kim, H.-M.; Yoo, S.-Y.; Roh, H.-S. A review on dry reforming of methane in aspect of catalytic properties. *Catal. Today* **2019**, *324*, 15-26.
- 6. Freund, H. J.; Roberts, M. W. Surface chemistry of carbon dioxide. *Surf. Sci. Rep.* **1996,** *25* (8), 225-273.
- 7. Wang, S.-G.; Liao, X.-Y.; Cao, D.-B.; Huo, C.-F.; Li, Y.-W.; Wang, J.; Jiao, H. Factors controlling the interaction of CO₂ with transition metal surfaces. *J. Phys. Chem. C* **2007**, *111* (45), 16934-16940.
- 8. Liu, C.; Cundari, T. R.; Wilson, A. K. CO₂ reduction on transition metal (Fe, Co, Ni, and Cu) surfaces: In comparison with homogeneous catalysis. *J. Phys. Chem. C* **2012**, *116* (9), 5681-5688.
- 9. Muttaqien, F.; Hamamoto, Y.; Inagaki, K.; Morikawa, Y. Dissociative adsorption of CO₂ on flat, stepped, and kinked Cu surfaces. *J. Chem. Phys.* **2014**, *141* (3), 034702.
- 10. Liu, X.; Sun, L.; Deng, W.-Q. Theoretical investigation of CO₂ adsorption and dissociation on low index surfaces of transition metals. *J. Phys. Chem. C* **2018**, *122* (15), 8306-8314.
- 11. Neugebohren, J.; Borodin, D.; Hahn, H. W.; Altschäffel, J.; Kandratsenka, A.; Auerbach, D. J.; Campbell, C. T.; Schwarzer, D.; Harding, D. J.; Wodtke, A. M.; Kitsopoulos, T. N. Velocity-resolved kinetics of site-specific carbon monoxide oxidation on platinum surfaces. *Nature* **2018**, *558* (7709), 280-283.
- 12. Zhou, L.; Kandratsenka, A.; Campbell, C. T.; Wodtke, A. M.; Guo, H. Origin of thermal and hyperthermal CO₂ from CO oxidation on Pt surfaces: The role of post-transition-state dynamics, active sites, and chemisorbed CO₂. *Angew. Chem. Int. Ed.* **2019**, *58* (21), 6916-6920.
- 13. D'Evelyn, M. P.; Hamza, A. V.; Gdowski, G. E.; Madix, R. J. Dynamics of the dissociative adsorption of CO₂ on Ni(100). *Surf. Sci.* **1986**, *167* (2–3), 451-473.
- 14. Lorraine, P. W.; Thoms, B. D.; Machonkin, R. A.; Ho, W. Translationally and vibrationally activated reaction of CO_2 on Si(111)7×7. *J. Chem. Phys.* **1992**, *96* (4), 3285-3297.
- 15. Jiang, B.; Guo, H. Communication: Enhanced dissociative chemisorption of CO₂ via vibrational excitation. *J. Chem. Phys.* **2016**, *144* (9), 091101.
- 16. Farjamnia, A.; Jackson, B. The dissociative chemisorption of CO₂ on Ni(100): A quantum dynamics study. *J. Chem. Phys.* **2017**, *146* (7), 074704.
- 17. Crim, F. F. Vibrational state control of bimolecular reactions: Discovering and directing the chemistry. *Acc. Chem. Res.* **1999**, *32*, 877-884.
- 18. Liu, K. Vibrational control of bimolecular reactcions with methane with mode-, bond-, and stereo-

- selectivity. Annu. Rev. Phys. Chem. 2016, 67, 91-111.
- 19. Juurlink, L. B. F.; Killelea, D. R.; Utz, A. L. State-resolve probes of methane dissociation dynamics. *Prog. Surf. Sci.* **2009**, *84*, 69-134.
- 20. Chadwick, H.; Beck, R. D. Quantum state—resolved studies of chemisorption reactions. *Annu. Rev. Phys. Chem.* **2017**, *68* (1), 39-61.
- 21. Smith, R. R.; Killelea, D. R.; DelSesto, D. F.; Utz, A. L. Preference for vibrational over translational energy in a gas-surface reaction. *Science* **2004**, *304* (5673), 992-995.
- 22. Jiang, B.; Yang, M.; Xie, D.; Guo, H. Quantum dynamics of polyatomic dissociative chemisorption on transition metal surfaces: Mode specificity and bond selectivity. *Chem. Soc. Rev.* **2016**, *45*, 3621-3640.
- 23. Zhou, X.; Kolb, B.; Luo, X.; Guo, H.; Jiang, B. Ab Initio molecular dynamics study of dissociative chemisorption and scattering of CO₂ on Ni(100): Reactivity, energy transfer, steering dynamics, and lattice effects. *J. Phys. Chem. C* **2017**, *121* (10), 5594-5602.
- 24. Luo, X.; Zhou, X.; Jiang, B. Effects of surface motion and electron-hole pair excitations in CO₂ dissociation and scattering on Ni(100). *J. Chem. Phys.* **2018**, *148* (17), 174702.
- 25. Burghaus, U. Surface chemistry of CO₂ Adsorption of carbon dioxide on clean surfaces at ultrahigh vacuum. *Prog. Surf. Sci.* **2014**, *89* (2), 161-217.
- 26. Jin, W.; Wang, Y.; Liu, T.; Ding, C.; Guo, H. CO₂ chemisorption and dissociation on flat and stepped transition metal surfaces. *Appl. Surf. Sci.* **2022**, *599*, 154024.
- 27. Viñes, F.; Borodin, A.; Höfft, O.; Kempter, V.; Illas, F. The interaction of CO₂ with sodium-promoted W(011). *Phys. Chem. Chem. Phys.* **2005**, *7* (22), 3866-3873.
- 28. Clavenna, L. R.; Schmidt, L. D. Decomposition of CO₂ on (100) W. Surf. Sci. 1972, 33 (1), 11-26.
- 29. Guo, H.; Jiang, B. The sudden vector projection model for reactivity: Mode specificity and bond selectivity made simple. *Acc. Chem. Res.* **2014**, *47* (12), 3679-3685.
- 30. Kresse, G.; Furthmuller, J. Efficient iterative schemes for ab initio total-energy calculations using plane wave basis set. *Phys. Rev. B* **1996**, *54*, 11169-11186.
- 31. Kresse, G.; Furthmuller, J. Efficiency of ab initio total energy calculations for metals and semiconductors using plane wave basis set. *Comp. Mater. Sci.* **1996**, *6*, 15-50.
- 32. Perdew, J. P.; Burke, K.; Ernzerhof, M. Generalized gradient approximation made simple. *Phys. Rev. Lett.* **1996**, *77*, 3865-3868.
- 33. Blöchl, P. E. Projector augmented-wave method. Phys. Rev. B 1994, 50, 17953-17979.
- 34. Henkelman, G.; Uberuaga, B. P.; Jónsson, H. A climbing image nudged elastic band method for finding saddle points and minimum energy paths. *J. Chem. Phys.* **2000**, *113* (22), 9901-9904.
- 35. Henkelman, G.; Jónsson, H. A dimer method for finding saddle points on high dimensional potential surfaces using only first derivatives. *J. Chem. Phys.* **1999**, *111* (15), 7010-7022.
- 36. Jiang, B.; Li, J.; Guo, H. Potential energy surfaces from high fidelity fitting of ab initio points: The permutation invariant polynomial-neural network approach. *Int. Rev. Phys. Chem.* **2016**, *35*, 479-506.
- 37. Behler, J. Perspective: Machine learning potentials for atomistic simulations. *J. Chem. Phys.* **2016**, 145 (17), 170901.
- 38. Jiang, B.; Li, J.; Guo, H. High-fidelity potential energy surfaces for gas phase and gas-surface scattering processes from machine learning. *J. Phys. Chem. Lett.* **2020**, *11* (13), 5120-5131.
- 39. Jiang, B.; Guo, H. Dynamics in reactions on metal surfaces: A theoretical perspective. *J. Chem. Phys.* **2019**, *150* (18), 180901.
- 40. Zhang, Y.; Hu, C.; Jiang, B. Embedded atom neural network potentials: Efficient and accurate machine learning with a physically inspired representation. *J. Phys. Chem. Lett.* **2019**, *10* (17), 4962-

4967.

- 41. Behler, J. Atom-centered symmetry functions for constructing high-dimensional neural network potentials. *J. Chem. Phys.* **2011**, *134*, 074106.
- 42. Zhou, X.; Zhang, Y.; Yin, R.; Hu, C.; Jiang, B. Neural network representations for studying gas-surface reaction dynamics: Beyond the Born-Oppenheimer static surface approximation. *Chin. J. Chem.* **2021**, *39* (10), 2917-2930.
- 43. Hase, W. L.; Duchovic, R. J.; Hu, X.; Komornicki, A.; Lim, K. F.; Lu, D.-H.; Peslherbe, G. H.; Swamy, K. N.; Linde, S. R. V.; Varandas, A.; Wang, H.; Wolf, R. J. VENUS96: A General Chemical Dynamics Computer Program. *Quantum Chemistry Program Exchange Bulletin* **1996**, *16*, 671.
- 44. Jiang, B.; Guo, H. Dynamics of water dissociative chemisorption on Ni(111): Effects of impact sites and incident angles. *Phys. Rev. Lett.* **2015**, *114*, 166101.
- 45. Guo, H.; Farjamnia, A.; Jackson, B. Effects of lattice motion on dissociative chemisorption: Toward a rigorous comparison of theory with molecular beam experiments. *J. Phys. Chem. Lett.* **2016**, *7*, 4576-4584.

Table I. SVP values for CO_2 dissociation on W(110) surface at the two transition states.

Mode	SVP	
	TS1	TS2
Vas	0.018	0.711
${oldsymbol{\mathcal{V}}_{ ext{SS}}}$	0.032	0.514
\mathcal{V} b	0.350	0.270
\boldsymbol{x}	0.041	0.140
y	0.038	0.107
z	0.886	0.016

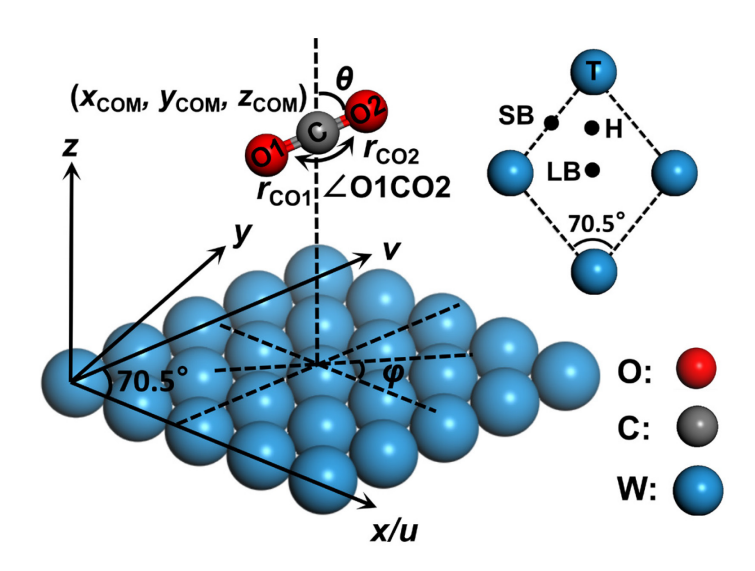


Figure 1. Jacobi coordinates for describing the process of CO₂ adsorption and dissociation on the pseudohexagonal W(110) surface. The inset shows the symmetry sites used in the system. T: top site, SB: short bridge site, LB: long bridge site, H: hollow site.

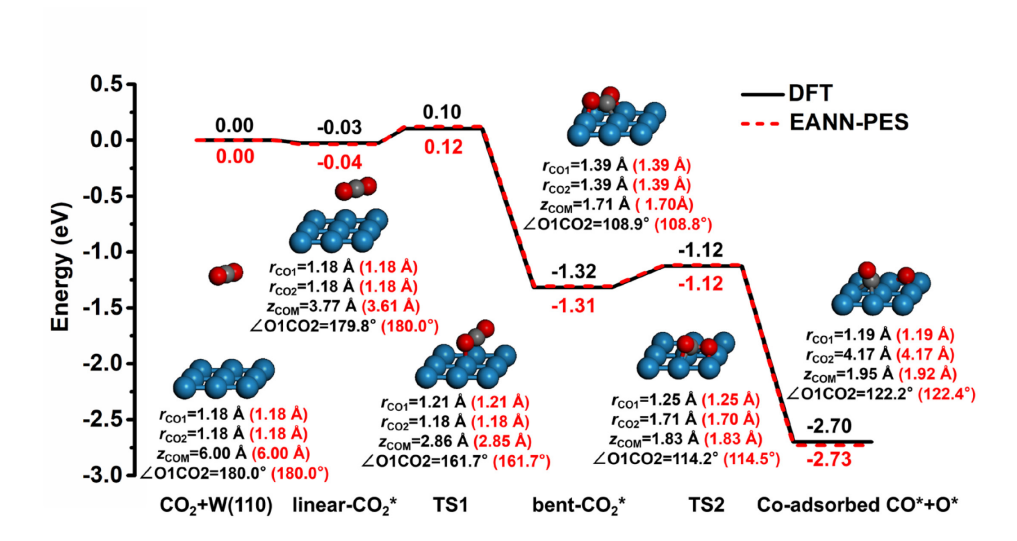


Figure 2. Comparison of geometries and energies (in eV) of adsorption minima, transition states and dissociative products in the minimum energy path of CO₂ dissociative chemisorption on the relaxed W(110) surface optimized directly with DFT (black) and with the EANN PES (red).

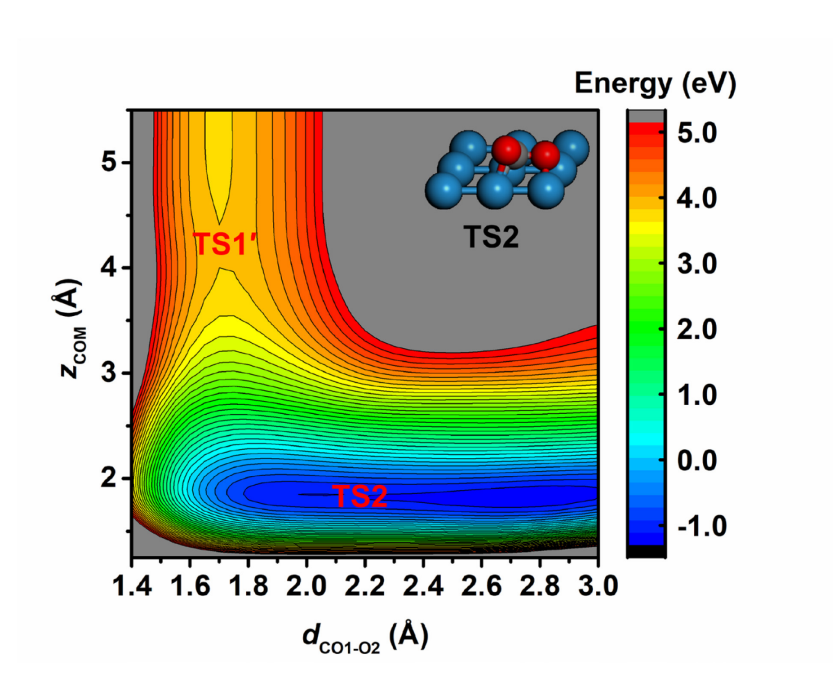


Figure 3. Two-dimensional contours of the EANN PES as a function of the CO1-O2 distance ($d_{\text{CO1-O2}}$) and the molecular height (z_{COM}) above the surface, with other coordinates fixed at the TS2.

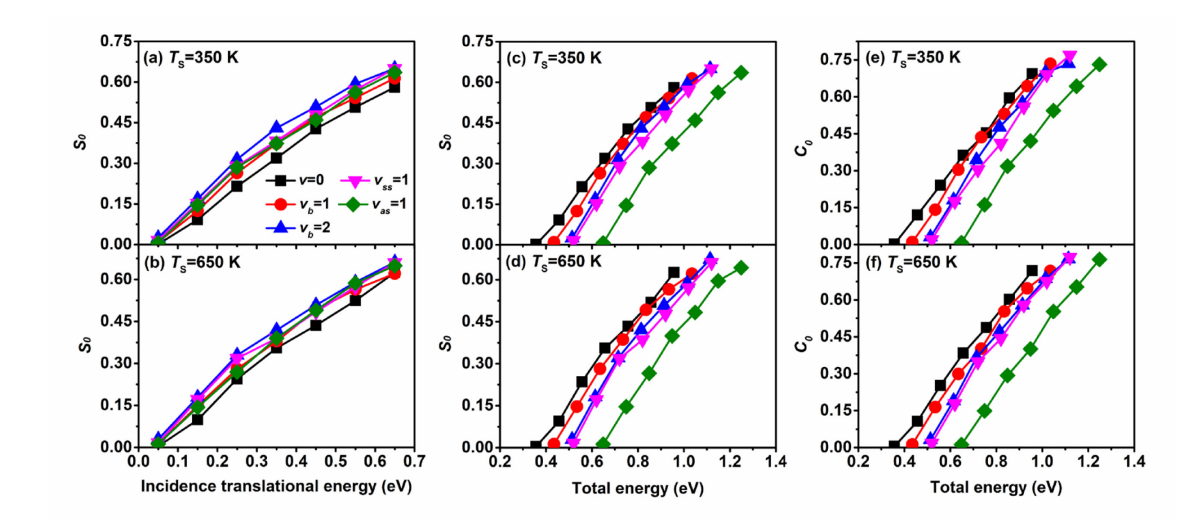


Figure 4. Calculated normal incident dissociative sticking probabilities (S_0) as a function of (a-b) incidence translational energy and (c-d) total energy at two different surface temperature, T_s =350 and 650 K for several CO₂ vibrational states. The total energy equals to the sum of the translational, rotational, and vibrational energy of the impinging CO₂. For comparison, the capture probabilities (C_0) are shown in (e-f) as a functional of total energy.

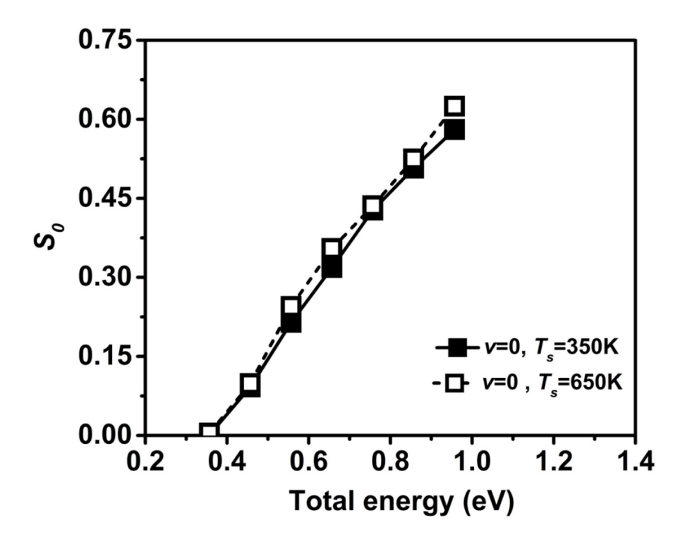


Figure 5. Calculated normal incident dissociative sticking probabilities (S_0) as a function of total energy at T_s equals to 350 and 650 K for the ground vibrational state of CO_2 .

TOC graphic

${\rm CO_2}$ dissociative chemisorption on W(110)

